ACS OMEGA

Open Access

http://pubs.acs.org/journal/acsodf

Article

CO_2 Adsorption on Biomass-Derived Carbons from *Albizia procera* Leaves: Effects of Synthesis Strategies

Aamir Hanif, Md. Abdul Aziz, Aasif Helal, Mahmoud M. Abdelnaby, Abuzar Khan, Rajesh Theravalappil, and Mohd Yusuf Khan*

Cite This: *ACS Omega* 2023, 8, 36228−36236

Read Online

ACCESS | Metrics & More | Article Recommendations

ABSTRACT: CO_2 capture is a useful strategy for controlling the risks associated with global warming. The design of an adsorbent is essential for clean and potentially energy-efficient adsorption-based carbon capture processes. This study reports a facile and moderately temperature single-stage combined pyrolysis and activation strategy for the synthesis of nitrogen-doped carbons for high-performance CO_2 capture. Using nitrogen-rich *Albizia procera* leaves as the precursor and carrying out single-stage pyrolysis and activation at temperatures of 500, 600, and 700 °C in the presence $NaHCO_3$ as an activating agent, carbons with different surface characteristics and ultrahigh weight percentage (22−25%) of nitrogen were obtained. The subtle differences in surface characteristics and nitrogen content had a bearing on the CO_2 adsorption performance of the resultant adsorbents. Outstanding results were achieved, with a CO_2 adsorption capacity of up to 2.5 mmol/g and a CO_2 over N_2 selectivities reaching 54. The isotherm results were utilized to determine the performance indicators for a practical vacuum swing adsorption process. This study provides a practical strategy for the efficient synthesis of nitrogen-doped carbons for various adsorption applications.

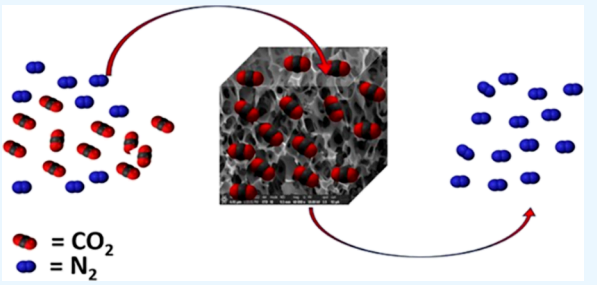

1. INTRODUCTION

Global warming is one of the most pressing issues of the 21st century, prompting international efforts to combat it.[1] Owing to the disruption of the natural equilibrium of CO_2 between various sources and sinks on earth, anthropogenic CO_2 emissions from fossil fuels are widely acknowledged as the primary cause of the exponential increase in atmospheric CO_2 levels.[2] Compared to a preindustrial revolution level of 278 ppm,[3] the current CO_2 level is 424 ppm (Mauna Loa Observatory. June 5, 2023), which is having severe consequences on the climate, including rising sea levels,[4] retreating glaciers,[5] and food scarcity.[6] Therefore, it is crucial to halt the increasing trend of CO_2 accumulation in the atmosphere.

Various short- to long-term solutions have been proposed, including using energy-efficient industrial technology and processes, switching to renewable energy sources, and sequestering CO_2.[7] However, it is not feasible to completely abandon fossil fuels in the near future. Carbon capture and sequestration are faster and more efficient methods for achieving sustainability.[8] Several methods, including chemical absorption,[9] membrane separation,[10] and solid adsorbent-based adsorption,[11] have been investigated for CO_2 capture. The effectiveness of the latter method depends on the composition of the adsorbent and is safe and potentially economical. The preferred adsorbents are those with high CO_2 adsorption capacity and selectivity, faster kinetics, facile regeneration, and the ability to be produced in large quantities on an economic scale.[12]

Materials such as zeolites,[13] MOFs,[14] alkali and alkaline metal oxide-based materials,[15] and functionalized silica[16] have been studied for CO_2 capture. Carbon generated from biomass has recently been highlighted as an economical and environmentally friendly alternative to synthetic adsorbents.[7] These carbons can be produced from readily available materials such as food, animals, and agricultural waste.[17] While the original CO_2 adsorption capacity (<0.5 mmol/g at 298 K and 1 bar) of pyrolyzed biomass is relatively low, several modifications are known to enhance its capacity and selectivity toward CO_2.[17] For example, doping with basic groups or heteroatoms, particularly nitrogen, enhances the alkalinity and CO_2 adsorption capacity of carbon.[18] Nitrogen doping is mainly achieved by treating carbon with a basic nitrogen-rich component or gas that introduces nitrogen atoms onto its surface.[19] Moreover, nitrogen-rich biomass precursors offer a

Received: July 1, 2023
Accepted: September 7, 2023
Published: September 21, 2023

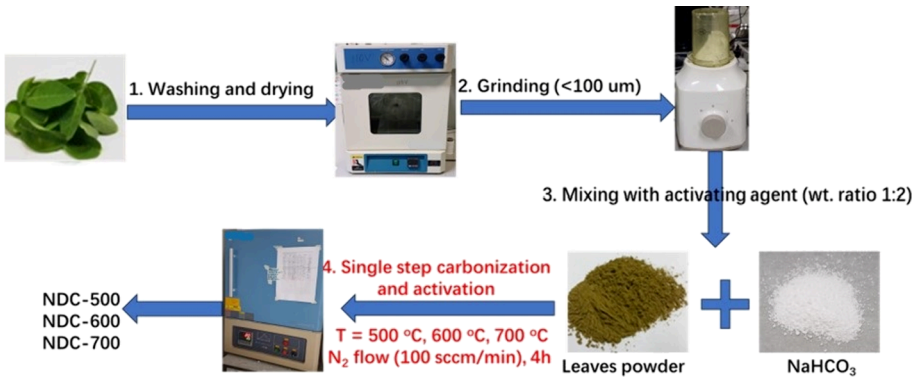

Figure 1. Synthesis scheme for the synthesis of carbons from *A. procera* leaves.

facile and more uniform method for nitrogen heteroatom doping. Additionally, enhancing the microporosity of carbon using various physical and chemical activation techniques is an effective strategy for improving its CO_2 adsorption performance. In particular, micropores <1 nm in diameter are highly effective for increasing the CO_2 capacity as they are close to the kinetic diameter of CO_2 and can interact with it via overlapping adsorption forces and potential fields from nearby pore walls.[20,21] Previous studies have used a post-synthesis activation method for carbon obtained from biomass to achieve a high level of microporosity. This involved utilizing CO_2 or steam as activating agents at temperatures between 500 and 900 °C to enhance micropore formation and boost CO_2 adsorption capabilities.[7] However, as carbon formation and activation involve a two-step process, they require significant time and energy. In addition, the temperature, flow rate, and synthesis equipment can affect the final porosity. Therefore, a simpler and more potent approach is required.

This study investigated a single-step carbonization and activation procedure utilizing *Albizia procera* leaves to create extremely microporous nitrogen-doped carbons with improved CO_2 adsorption properties. *A. procera* grows in several regions, including the Middle East and Southeast Asia.[22] Leaf biomass is rich in crude protein,[22] which serves as a source of nitrogen during leaf pyrolysis. After washing, drying, and pulverizing, the leaf biomass was mixed with $NaHCO_3$ and carbonized at different temperatures. $NaHCO_3$ was used as an activator to generate CO_2 and steam during the synthesis without the need for a continuous external supply of these gases. This enabled the production of microporous carbon via a single-step pyrolysis and activation process. The resulting materials were subjected to unary isotherms for CO_2 and N_2 at various temperatures, and their regeneration capabilities and selectivity for CO_2 over N_2 were evaluated. Finally, the vacuum swing adsorption (VSA) performance of the adsorbents was comprehensively evaluated.

2. EXPERIMENTAL SECTION

2.1. Materials. Leaves from *A. procera* were collected from the university compound of King Fahad University of Petroleum and Minerals, Dhahran, Saudi Arabia. $NaHCO_3$ (99.7%, Sigma-Aldrich), N_2 (99.99% purity, SCG Gas, Saudi Arabia), and deionized water were also used during the synthesis.

2.2. Preparation of Nitrogen-Doped Carbons (NDCs). A general scheme of the synthesis of carbons from *A. procera* leaves is given in Figure 1. *A. procera* leaves were first washed with deionized water followed by sun drying for 2 days until the leaves developed a crispy texture. These leaves were then further dried under controlled conditions in a forced air convection oven set at 100 °C for approximately 2 days. The leaves were pulverized into a fine powder using a kitchen blender. After the powder was sieved through a mesh of 100 μm, 3 g of the leaf powder was mixed with 6 g of $NaHCO_3$ and homogenized in a blender for 5 min. Next, the mixture was subjected to different pyrolysis temperatures of 500, 600, and 700 °C under flowing N_2 for 5 h. The final pyrolysis temperatures were achieved at a rate of 10 °C/min, and after the completion of the dwell time, the samples were cooled down in a controlled manner with a ramp down rate of 5 °C/min under flowing N_2. Once the temperature reached below 50 °C, the samples were removed and washed with 100 mL of 1 M HCl in an ultrasonic bath for 20 min. The samples were recovered via centrifugation and washed three times with deionized water over a filter paper. Finally, the samples were dried at 60 °C in an oven for 24 h. The samples were labeled as NDC-500, NDC-600, and NDC-700, with the numbers indicating the pyrolysis temperature in °C.

2.3. Characterization. The synthesized materials were characterized by using various techniques to elucidate their physicochemical and surface properties. Powder X-ray diffraction was conducted using a Rigaku Miniflex-II diffractometer fitted with a Cu−Kα anode (λ= 0.15416 nm) within the range of 5−70° at a scan rate of 2°/min and a step size of 0.02°. Fourier transform infrared (FTIR) scans in the range of 4000−650 cm^{-1} were collected using a Nicolet 6700 spectrometer (Thermo Fisher Scientific, USA) for functional group identification. SEM micrographs were obtained using high-resolution field-emission scanning electron microscopy (FE-SEM; TESCAN-LYRA-3, Czech Republic). The SEM samples were prepared by dispersing them in ethanol and mounting them on copper tape. SEM-EDX measurements were performed on the same instrument by using an Oxford Aztec Energy X-MAX 50 EDS system. Raman spectra were collected in the range of 800−2000 cm^{-1} using an iHR320 HORIBA Raman spectrometer. XPS analysis was carried out using a thin carbon layer dispersed on fluorine-doped tin oxide glass slides using an ESCALAB 250Xi Thermo Scientific spectrometer. Information about the surface area and pore size distribution was obtained by performing N_2 adsorption measurements at −196.15 °C using a Quadrasorb SI instrument (Quantachrome Instruments, U.S.). For the sample preparation and pretreatment, 100−200 mg of the sample was degassed at 130 °C for 24 h under a high dynamic vacuum

https://doi.org/10.1021/acsomega.3c04693
ACS Omega 2023, 8, 36228−36236

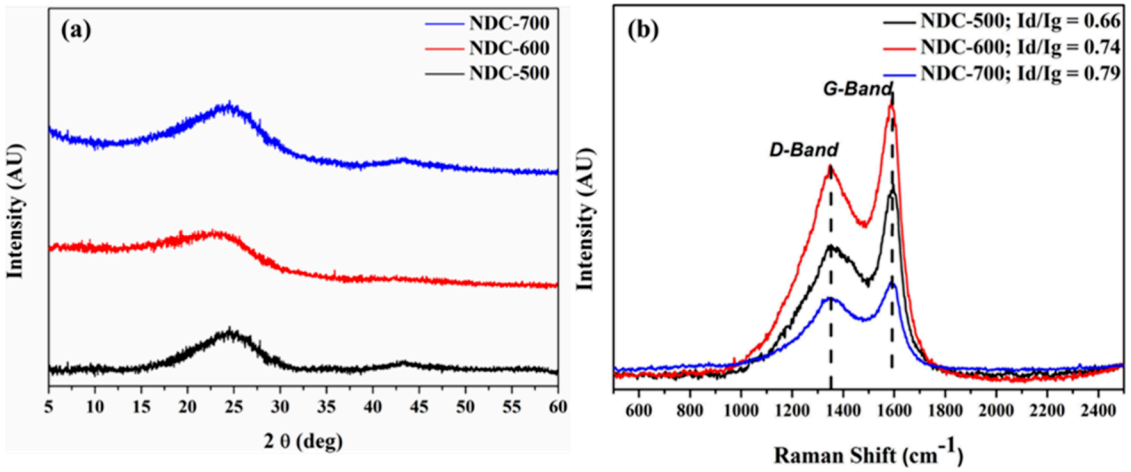

Figure 2. (a) PXRD patterns and (b) Raman spectra of NDCs.

(10^{-5} bar). Elemental (CHN) analysis was carried out using a PerkinElmer Series II CHN 2400 analyzer.

2.4. CO_2 and N_2 Isotherm Measurements. Single-component CO_2 and N_2 isotherms of the nitrogen-doped carbons (NDCs) at 0 and 25 °C were conducted using a Quadrasorb SI instrument (Quantachrome Instruments, U.S.). Approximately 200 mg of the samples was pretreated at 130 °C under vacuum for 24 h before being weighed again. This was followed by an additional 2 h of in situ degassing at 70 °C under a dynamic vacuum. The target temperatures for the isotherm measurements were maintained using a water circulation bath containing a 1:1 mixture of water and ethylene glycol. The experimental data points were fitted with the Langmuir and dual-site Langmuir models to elucidate the adsorption mechanism.[23] From the isotherm adsorption capacities, the following parameters determining the adsorbent performance for a practical VSA (vacuum swing adsorption) process operating between 1 and 0.1 bar pressure were calculated using eqs 1−4.[24]

$$\text{CO}_2\text{working capacity, (mmol/g)} W_{CO2} = n_{CO2}^{ads} - n_{CO2}^{des} \quad (1)$$

$$\text{regenerability (\%)}\ R = \left(\frac{W_{CO2}}{n_{CO2}^{ads}}\right) \times 100 \quad (2)$$

$$\text{selectivity, } \alpha_{CO2/N2} = \left(\frac{n_{CO2}^{ads}}{n_{N2}^{ads}}\right)\left(\frac{p_{N2}}{p_{CO2}}\right) \quad (3)$$

$$\text{sorbent selection parameter } (S) = ((\alpha_{CO2/N2}^{ads})^2/(\alpha_{CO2/N2}^{des})) \times (W_{CO2}/W_{N2}) \quad (4)$$

where n_{CO2}^{ads} (mmol/g) is the CO_2 capacity obtained from the adsorption isotherm at 1 bar, n_{CO2}^{des} is the capacity obtained from the desorption arm of the isotherm at 0.1 bar, and p_{N2} and p_{CO2} are the partial pressures of N_2 and CO_2, respectively, in model post-combustion feed gases of 15% CO_2 and 85% N_2.

3. RESULTS AND DISCUSSION

3.1. Preparation of NDCs. Nitrogen doping and enhancement of the micropore density of carbon are two major strategies for enhancing the CO_2 adsorption performance of carbon-based materials. Nitrogen serves as a basic group within the carbon network, thereby enhancing its interaction with CO_2, which is of an acidic nature. Meanwhile, micropores, typically <1 nm in size, provide stronger interaction with CO_2 molecules because their size is close to that of the kinetic diameter of CO_2, enabling better interaction via overlapping adsorption forces and potential fields from nearby pore walls. Conventionally, nitrogen groups are introduced into carbon materials using two strategies: (i) post-treatment of the synthesized carbons with additional basic nitrogen-rich chemical agents or gases, which then introduces surface nitrogen heteroatoms over the carbon. (ii) Heteroatom self-doping, where the carbon precursor reacts with the nitrogen precursor and is then subjected to pyrolysis to afford a uniform dispersion of nitrogen over the carbons. However, both of these nitrogen doping strategies rely on synthetic precursors and a multistep synthesis scheme, which adds complexity to the process and makes it economically unattractive. Furthermore, to introduce micropores, a post-synthesis treatment with steam or CO_2 is generally performed. The carbons obtained via the pyrolysis of biomass are exposed to CO_2 or steam at a high temperature (500−900 °C).[7,25] The dissociative chemisorption of CO_2 occurs on carbon, resulting in the formation of surface oxides and CO, which are subsequently released from the surface and aid in the formation of micropores.[26] In steam modification, the reactive centers dissociate water molecules, forming a bond with oxygen and releasing H_2, which forms transient hydrogen complexes on the surface. These surface complexes are finally released, leaving carbon in a highly porous state.[27] However, steam and CO_2 post-synthesis activation strategies suffer from notable disadvantages, including the requirement for a two-step preparation process, continuous supply of high-purity CO_2 and steam at high temperatures for several hours, and nonuniform exposure of the material to the activating gas. These factors contribute to the reduced efficiency and questionable reproducibility of the activation process. To address these limitations, a biomass precursor with an inherently high nitrogen content was carefully selected to produce nitrogen-doped carbons. Moreover, a single-step carbonization−activation procedure was used in this study, which involves the in situ generation of CO_2 and H_2O via the thermal decomposition of $NaHCO_3$ according to the following reactions:[28]

https://doi.org/10.1021/acsomega.3c04693
ACS Omega 2023, 8, 36228−36236

$$2NaHCO_3 \rightarrow Na_2CO_3 + CO_2(g) + H_2O(g) \quad (5)$$

$$Na_2CO_3 \rightarrow Na_2O + CO_2(g) \quad (6)$$

By adjustment of the pyrolysis conditions, the activation potential of CO_2 and steam (H_2O) could be utilized during the carbonization step without the need for a continuous external supply of these gases. This procedure also addresses the nonuniform exposure of carbon to the activating agent. Therefore, adsorbents prepared using this facile synthesis strategy are expected to exhibit a high CO_2 capture performance.

3.2. Characterization of NDCs. The physicochemical and surface characteristics of the adsorbents closely control their ability to adsorb gases. The adsorbents were thoroughly evaluated using a variety of methodologies to understand the effects of various preparation factors on the adsorbent characteristics and consequent CO_2 capture ability. Figure 2a shows the XRD patterns of all of the NDCs. Poor crystalline solid and low degree of graphitization are indicated by a large hump at approximately 2θ = 25−29°. Thus, it can be concluded that these materials are primarily amorphous because all the samples exhibit comparable XRD results without any clearly defined peaks. The Raman spectra of the materials (Figure 2b) also indicated a disordered nature. The two bands at 1580 and 1350 cm^{-1} are referred to as the D- and G-bands, respectively. The G-band indicates the sp^2 C−C bond in-plane stretching and the graphitic nature of carbon. In contrast, the D-band signifies a peak of disorder in the A_{1g} vibrational mode, indicating defects in the graphitic lattice.[29] The intensity ratio of the D- and G-bands (I_d/I_g ratio) in the XRD results was further supported by the Raman spectra of the materials (Figure 2b). The intensity ratio of the D- and G-bands indicates defects in carbon-based materials, with higher I_d/I_g ratios indicating higher defect intensity. A ratio approaching zero indicates a predominantly ordered graphitic structure.[30] As indicated by the I_d/I_g ratios, the NDC materials exhibited disorder, which continued to increase with increasing pyrolysis temperature. Figure 3 depicts the FTIR plots of the NDCs obtained to examine the effect of the pyrolysis temperature on the surface functionalization of carbons. In agreement with previously reported IR peak assignments, the broad peak around 3381 cm^{-1} was attributed to −OH stretching[31] whereas peaks centered around 1580 and 1623 cm^{-1} were indicative of −C═C− stretching.[32] The peak at approximately 1420 cm^{-1} indicates −CO stretching.[33] Moreover, the minor peaks at around 876 cm^{-1} are attributed to surface −CH groups. XPS analysis (Figure 4) of a representative sample (NDC-600) also supports FTIR results. The overall survey scan for sample NDC-600 is shown in Figure 4a. Further deconvolution of the C 1s peak (Figure 4b) indicates aromatic character (−C═C− at 284.3 eV and −C−C− at 285.3 eV bonds) as well as the presence of C−O/C−OH (288.4 eV) functionalities.[7,34]

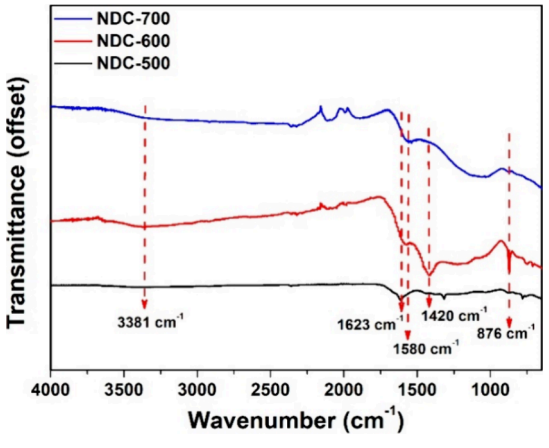

Figure 3. FTIR spectra of NDCs.

Similarly, deconvolution of the N 1s peak shows the presence of both pyrrolic and pyridinic nitrogen corresponding to binding energies of 400 s and 398.4 eV, respectively.[34] Figure 5a−c shows the FE-SEM micrographs of the synthesized NDCs at 500, 600, and 700 °C, respectively. A porous foam-type morphology formed by an intricately interconnected network of perforated nanosheets was observed. At higher pyrolysis temperatures, the pore morphology was clearly visible, possibly because of the complete pyrolysis of the precursor. Further, EDX results (Figure 6a−c) show the presence of approximately 18−24 wt % nitrogen in the NDC samples, confirming the successful doping of nitrogen heteroatoms in the carbon samples.

CHN analysis was carried out to further precisely determine the composition of the synthesized adsorbents. As indicated in Table 1, the nitrogen content of the samples ranges from 21 to 27% with NDC-600 exhibiting the highest nitrogen doping percentage, which could lead to the formation of stronger bonds with CO_2 due to acid−base interactions. Further, elemental mapping of the NDC samples confirms the uniform distribution of nitrogen on carbons (Figure 7).

The pyrolysis temperature is known to affect the surface area and pore characteristics of synthesized adsorbents, which in turn are important for gas uptake. To examine the surface and porosity characteristics, we measured N_2 adsorption isotherms at the temperature of liquid nitrogen (−196.15 °C). Figure 8a shows the pseudotype-II isotherms with a narrow H3 hysteresis loop, which is indicative of both microporosity and mesoporosity in the sample.[35] This was also supported by the DFT pore size distribution (Figure 8b), which indicated a predominance of microporosity and some mesoporosity. Additionally, different amounts of N_2 sorption indicated varying surface areas of the samples in the order of NDC-700 > NDC-600 > NDC-500. Furthermore, NDC-700 had a narrow micropore size distribution centered around 5 Å, whereas NDC-500 and NDC-600 had relatively broad pore size distributions. Table 2 shows the Brunauer−Emmett−Teller (BET) surface area and porosity measurements acquired from N_2 adsorption at −196.15 °C. The NDC-700 sample had the highest surface area, total pore volume, and micropore volume followed by NDC-600 and NDC-500.

However, the average pore diameter exhibited an inverse trend, indicating a decrease from JDC-700 to JDC-600 to JDC-500. This suggests that, all other factors being held equal, a higher pyrolysis temperature yields a significantly larger surface area and an increased proportion of micropore volume, both of which are known to promote CO_2 adsorption onto carbon.

3.3. CO_2 and N_2 Adsorption Performance. The potential of NDCs to adsorb and separate CO_2 from N_2 was evaluated by measuring the adsorption and desorption isotherms of N_2 and CO_2 at temperatures of 0 and 25 °C within a pressure range of 0−1 bar. The CO_2 adsorption capacity at 1 bar ranged from 0.76 to 2.53 mol/kg across the measured temperatures (Figure 9b,c). NDC-700 exhibited the

https://doi.org/10.1021/acsomega.3c04693
ACS Omega 2023, 8, 36228−36236

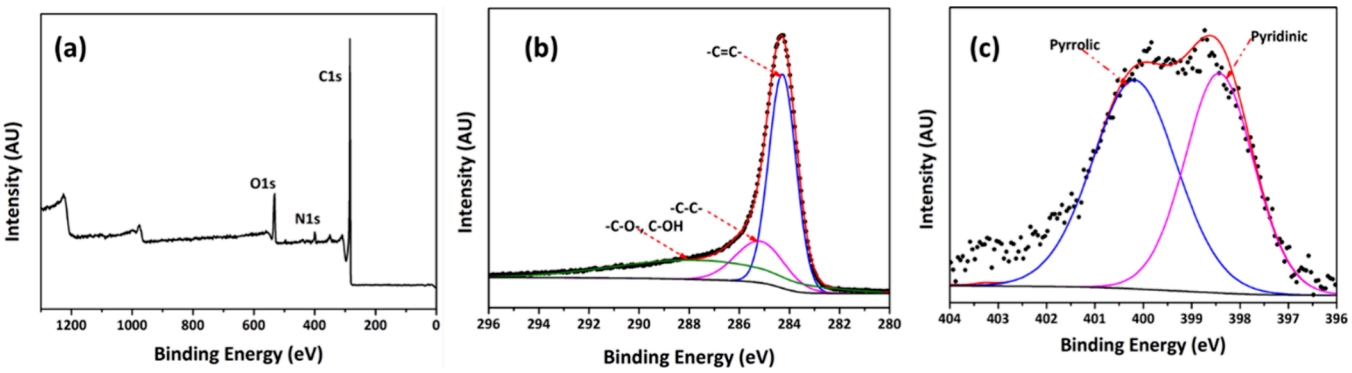

Figure 4. XPS images of NDC-600. (a) Survey scan, (b) C 1s peak, and (c) N 1s peak.

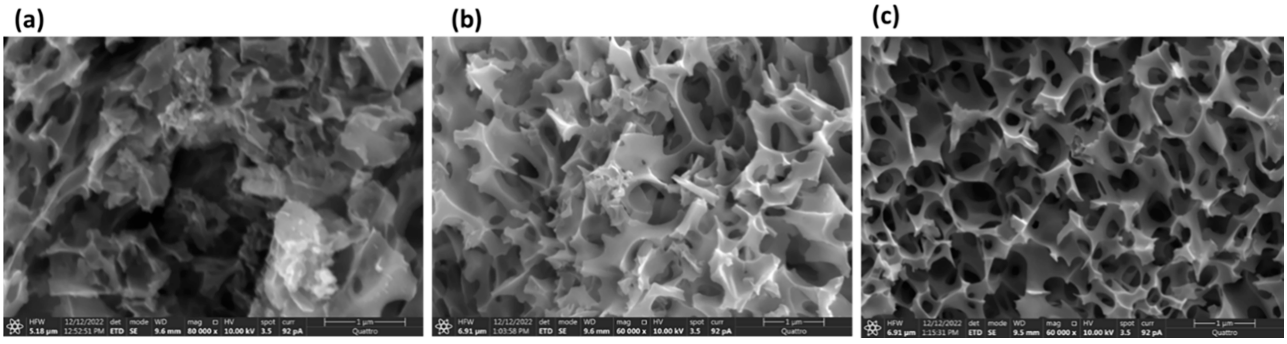

Figure 5. FE-SEM micrographs of NDCs: (a) NDC-500, (b) NDC-600, and (c) NDC-700.

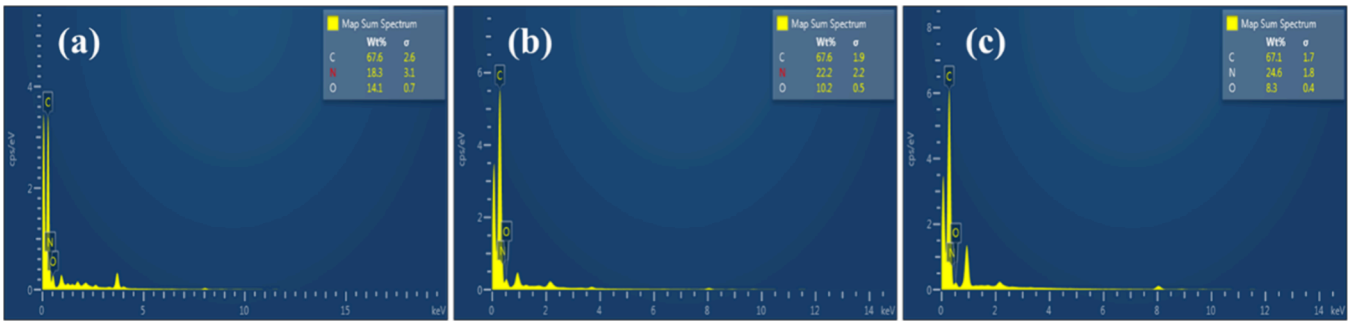

Figure 6. EDX plots of NDCs: (a) NDC-500, (b) NDC-600, and (c) NDC-700.

Table 1. Elemental Percentage of NDC Samples from CHN Analysis

sample	C (%)	H (%)	N (%)
NDC-500	71.8	3.4	24.8
NDC-600	68.2	4.2	27.6
NDC-700	77.1	1.4	21.6

highest CO_2 adsorption capacity followed by NDC-600. Meanwhile, NDC-500 exhibited the lowest capacity among the three samples for both temperatures (0 and 25 °C). For the same adsorbent, the capacity at 0 °C was higher than that at 25 °C. Further, as indicated by the hollow star symbols, all the materials had an overlapping desorption arm of the isotherms. These trends showed a positive correlation with the surface area and pore volume of the NDCs, which is consistent with previous studies.[24,36] However, despite having a smaller surface area than other reported carbon-based adsorbents, these materials exhibited significant CO_2 uptake. This can be attributed to the presence of nitrogen heteroatoms, which increased the alkalinity of the adsorbents. In addition, narrow-tailored micropores with diameters of less than 1 nm facilitated interactions between CO_2 and the adsorbent.[20] Furthermore, the CO_2 capacity was further enhanced by hydroxyl and aromatic functional groups via acid−base and $\pi-\pi$ interactions, respectively.[13,37] Notably, these results are among the highest adsorption capacities reported for biomass-derived hydrocarbons (Table 3). The isotherm model fitting of the experimental data revealed that the DSL model provided a better fit than the Langmuir model, as indicated by its lower sum of squared error (SSE) fitness parameter (Figure 9a). This indicates two different types of adsorption sites with varying interactions with the adsorbate molecules. Subsequently, all other isotherms in this study were fitted using the DSL model (Figures 9b and 7c). The CO_2 over N_2 selectivity of a representative post-combustion capture mixture (15% CO_2 and 85% N_2) is shown in Figure 9d. The selectivities of the adsorbent ranged from 17 to 112 at the studied pressures and temperatures, highlighting their potential for CO_2-N_2

https://doi.org/10.1021/acsomega.3c04693
ACS Omega 2023, 8, 36228−36236

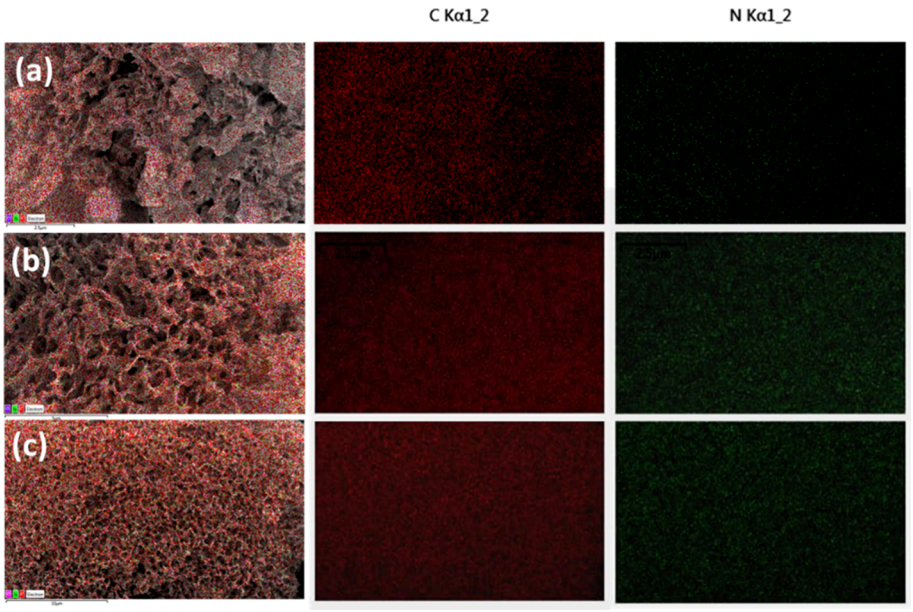

Figure 7. Elemental mapping of NDC samples: (a) NDC-500, (b) NDC-600, and (c) NDC-700.

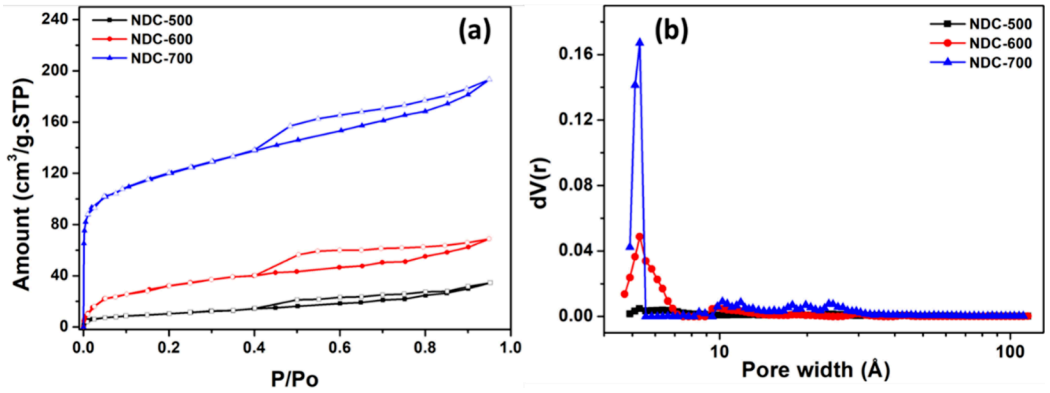

Figure 8. (a) N_2 adsorption isotherms at −196.15 °C and (b) DFT pore size distribution of adsorbents.

Table 2. Surface Area and Porosity Characteristics of the NDCs[a]

sample code	S_{BET} (m^2/g)	V_{tot} (cm^3/g)	V_{mi} (cm^3/g)	$\%_{mi}$(%)	D_{av}(nm)
NDC-500	39	0.046	0.024	52.17	2.4
NDC-600	118	0.097	0.045	46.39	1.6
NDC-700	426	0.28	0.177	63.21	1.32

[a] S_{BET} = BET surface area, V_{tot} = total pore volume calculated at P/P_o = 0.95, V_{mi} = HK micropore volume, $\%_{mi} = (V_{mi}/V_{tot}) \times 100$, and D_{av}= average pore diameter.

separation. Furthermore, the selectivity at 0 °C was greater than that at 25 °C for all of the adsorbents.

3.4. CO_2−N_2 Separation Performance Indicators of NDCs in the Cyclic Vacuum Swing Adsorption Process. VSA is a well-established cyclic process that utilizes various gas separation processes and provides energy-efficient gas separation with automatic control. However, it may not be feasible to use large quantities of adsorbents in VSA when evaluating adsorbents on a laboratory scale. Isotherms provide a reasonable indication of the suitability of an adsorbent for full-scale VSA processes.[24] Thus, we calculated some of the important indicators of VSA performance from the isotherm results, as shown in Table 4. For example, the actual usable capacity in the VSA process is called the working capacity, and a higher working capacity is preferred. NDC-700 exhibited the highest working capacity among all the adsorbents at both 0 and 25 °C. However, the working capacity is not the sole indicator of VSA performance. Despite having a better working capacity, a lower CO_2 over N_2 selectivity may limit the application of the absorbent. NDC-600 has the best selectivity at 1 bar and 0 °C and almost the same selectivity as that of NDC-700 at 25 °C, which in turn is higher than that of NDC-500. Thus, considering its selectivity, NDC-600 can be regarded as the best adsorbent. Regenerability is another factor to consider when determining the suitability of adsorbents for VSA processes as it indicates the ability of the adsorbent to be reused in cyclic experiments. All the NDCs exhibited a good regenerability of approximately 60−70%. Because there is no single indicator to determine the suitability of adsorbents for the VSA process, researchers have devised a unified parameter called the sorbent selection parameter (S), which considers the working capacity, selectivity, and regenerability to provide a single empirical value for comparison. Higher S values indicate the greater suitability of a particular VSA process under the given conditions. Despite

https://doi.org/10.1021/acsomega.3c04693
ACS Omega 2023, 8, 36228−36236

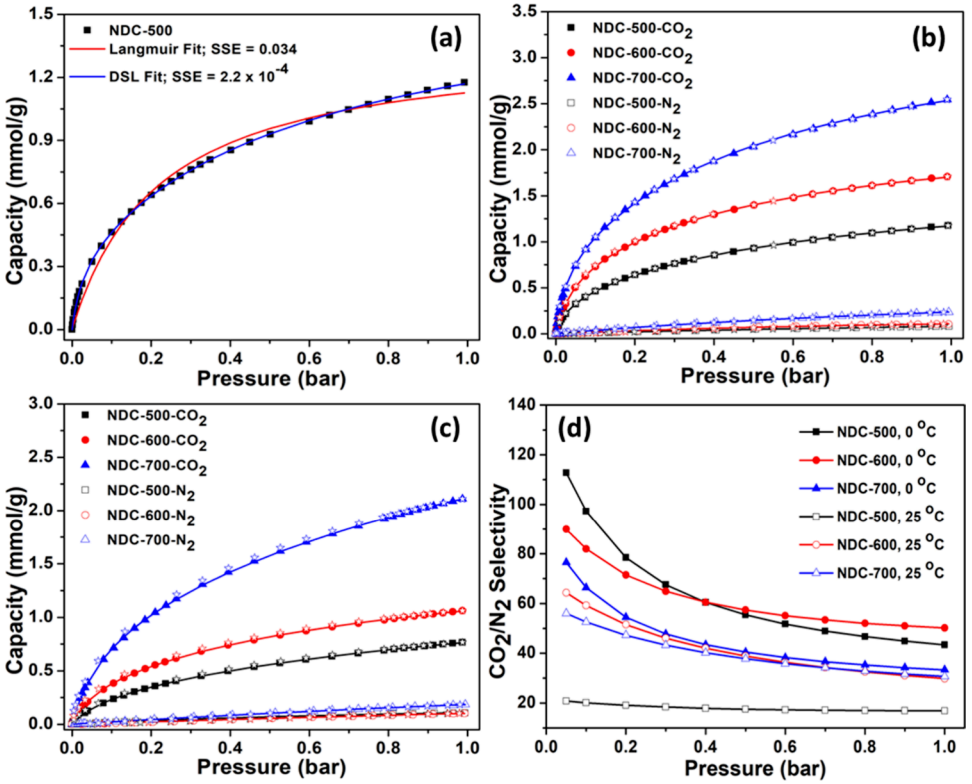

Figure 9. (a) Langmuir and dual-site Langmuir fitting of the NDC-500 isotherm at 0 °C. (b) CO_2 and N_2 isotherms of adsorbents at 0 °C. Points represent the experimental data, and hollow star symbols represent desorption data of each isotherm and line DSL fit. (c, d) CO_2 and N_2 isotherms of adsorbents at 25 °C. Points represent the experimental data, and hollow star symbols represent desorption data of each isotherm and line DSL fit.

Table 3. CO_2 Capacities of Different Biomass-Derived Carbons Reported in the Literature

biomass type	pyrolysis temperature (°C)	activating agent	adsorption temperature (°C)	CO_2adsorption capacity (mmol/g)	reference
paper mill sludge	300	none	25	0.18	7
paper mill sludge	600	none	25	0.31	7
pine saw dust	550	none	25	1.67	7
pine saw dust	550	steam	25	1.74	7
bagasse and hickory chips	600	NH_4OH	25	1.18	38
cotton stalk	800	CO_2	20	2.25	39
vine shoot	600−800	CO_2	25	1.58	40
coffee ground	600	MgO	25	1.57	41
Populus nigra wood	700	steam	25	1.12	42
oak biomass	700	K_2CO_3 + Na_2CO_3 + Li_2CO_3	25	1.65	36
hickory wood	600		25	1.04	43
bamboo charcoal[a]	1000 and 700	KOH	25	3.38	44
A. procera leaves	700	$NaHCO_3$	0	2.54	this work
A. procera leaves	700	$NaHCO_3$	25	2.11	this work

[a]Synthesized in two stages, bamboo sawdust is first pyrolyzed at 1000 °C and activated at 700 °C.

Table 4. CO_2−N_2 Separation Performance Indicators for a VSA Process Operating between 0.1 and 1 bar

sample code	temperature (°C)	CO_2working capacity (W)(mmol/g)	selectivity$_{CO2/N2}$	regenerability	sorbent selection parameter (S)
NDC-500	0	0.71	43	61	193
NDC-600	0	0.98	50	58	331
NDC-700	0	1.50	33	60	130
NDC-500	25	0.53	17	66	85
NDC-600	25	0.73	30	69	123
NDC-700	25	1.39	31	66	160

https://doi.org/10.1021/acsomega.3c04693
ACS Omega 2023, 8, 36228−36236

its lower working capacity, NDC-600 is the best choice for VSA at 0 °C, while NDC-700 performs well at 25 °C.

4. CONCLUSIONS

High-performance nitrogen-doped carbon was derived via the moderate temperature single-step pyrolysis and activation of *A. procera* leaves containing an ultrahigh percentage of nitrogen. By careful choice of precursor, activation agent, and activation temperature, a narrow micropore size distribution was obtained for the synthesized carbons with a high level of nitrogen doping. The synthesized carbons exhibited a high percentage of nitrogen doping, hydroxyl groups, and aromatic rings, resulting in a high CO_2 capacity and good CO_2/N_2 selectivity. An appreciable CO_2 adsorption capacity of up to 2.54 mmol along with appreciable CO_2/N_2 selectivity (33) was exhibited by NDC-700 at 0 °C. However, given their higher nitrogen content than NDC-700, NDC-500 and NDC-600 exhibited even higher CO_2/N_2 selectivities of 43 and 50, respectively, despite a lower adsorption CO_2 adsorption capacity than NDC-700. Thus, for a comprehensive comparison, the sorbent selection parameters were calculated by considering the working capacity, regenerability, and selectivity of the adsorbents. Based on the sorbent selection parameters, NDC-600 exhibited the best CO_2/N_2 separation performance at 0 °C, while NDC-700 performed better at 25 °C for CO_2–N_2 VSA. These materials and synthesis strategies can be applied to a wide range of acid gas capture applications.

AUTHOR INFORMATION

Corresponding Author

Mohd Yusuf Khan − *Interdisciplinary Research Center for Hydrogen and Energy Storage (IRC-HES), King Fahd University of Petroleum & Minerals, Dhahran 31261, Saudi Arabia;* orcid.org/0000-0002-1199-6232; Email: mykhan@kfupm.edu.sa

Authors

Aamir Hanif − *Interdisciplinary Research Center for Hydrogen and Energy Storage (IRC-HES), King Fahd University of Petroleum & Minerals, Dhahran 31261, Saudi Arabia*

Md. Abdul Aziz − *Interdisciplinary Research Center for Hydrogen and Energy Storage (IRC-HES), King Fahd University of Petroleum & Minerals, Dhahran 31261, Saudi Arabia;* orcid.org/0000-0002-1537-2785

Aasif Helal − *Interdisciplinary Research Center for Hydrogen and Energy Storage (IRC-HES), King Fahd University of Petroleum & Minerals, Dhahran 31261, Saudi Arabia;* orcid.org/0000-0003-2013-5327

Mahmoud M. Abdelnaby − *Interdisciplinary Research Center for Hydrogen and Energy Storage (IRC-HES), King Fahd University of Petroleum & Minerals, Dhahran 31261, Saudi Arabia;* orcid.org/0000-0003-3434-8593

Abuzar Khan − *Interdisciplinary Research Center for Hydrogen and Energy Storage (IRC-HES), King Fahd University of Petroleum & Minerals, Dhahran 31261, Saudi Arabia;* orcid.org/0000-0001-9122-2247

Rajesh Theravalappil − *Center for Refining and Advanced Chemicals, King Fahd University of Petroleum & Minerals, Dhahran 31261, Saudi Arabia*

Complete contact information is available at: https://pubs.acs.org/10.1021/acsomega.3c04693

Notes

The authors declare no competing financial interest.

ACKNOWLEDGMENTS

The authors greatly acknowledge the support provided by the Deanship of Research Oversight and Coordination (DROC) and the Interdisciplinary Research Center for Hydrogen and Energy Storage (IRC-HES) for funding this work through project number INHE2103 at King Fahd University of Petroleum and Minerals (KFUPM).

REFERENCES

(1) Fawzy, S.; Osman, A. I.; Doran, J.; Rooney, D. W. Strategies for mitigation of climate change: a review. *Environ. Chem. Lett.* **2020**, *18*, 2069−2094.

(2) Devi, S.; Gupta, N. Dynamics of carbon dioxide gas (CO2): Effects of varying capability of plants to absorb CO2. *Nat. Res. Model.* **2019**, *32* (1), No. e12174.

(3) Hamieh, A.; Rowaihy, F.; Al-Juaied, M.; Abo-Khatwa, A. N.; Afifi, A. M.; Hoteit, H. Quantification and analysis of CO2 footprint from industrial facilities in Saudi Arabia. *Energy Convers. Manage.: X* **2022**, *16*, No. 100299.

(4) Meehl, G. A.; Washington, W. M.; Collins, W. D.; Arblaster, J. M.; Hu, A.; Buja, L. E.; Strand, W. G.; Teng, H. How much more global warming and sea level rise? *Science* **2005**, *307* (5716), 1769−1772.

(5) Oerlemans, J. Quantifying global warming from the retreat of glaciers. *Science* **1994**, *264* (5156), 243−245.

(6) Wheeler, T.; Von Braun, J. Climate change impacts on global food security. *Science* **2013**, *341* (6145), 508−513.

(7) Igalavithana, A. D.; Choi, S. W.; Shang, J.; Hanif, A.; Dissanayake, P. D.; Tsang, D. C. W.; Kwon, J. H.; Lee, K. B.; Ok, Y. S. Carbon dioxide capture in biochar produced from pine sawdust and paper mill sludge: Effect of porous structure and surface chemistry. *Sci. Total Environ.* **2020**, *739*, No. 139845.

(8) Bui, M.; Adjiman, C. S.; Bardow, A.; Anthony, E. J.; Boston, A.; Brown, S.; Fennell, P. S.; Fuss, S.; Galindo, A.; Hackett, L. A.; Hallett, J. P.; Herzog, H. J.; Jackson, G.; Kemper, J.; Krevor, S.; Maitland, G. C.; Matuszewski, M.; Metcalfe, I. S.; Petit, C.; Puxty, G.; Reimer, J.; Reiner, D. M.; Rubin, E. S.; Scott, S. A.; Shah, N.; Smit, B.; Trusler, J. P. M.; Webley, P.; Wilcox, J.; Mac Dowell, N. Carbon capture and storage (CCS): the way forward. *Energy Environ. Sci.* **2018**, *11* (5), 1062−1176.

(9) Ochedi, F. O.; Yu, J.; Yu, H.; Liu, Y.; Hussain, A. Carbon dioxide capture using liquid absorption methods: a review. *Environ.Chem. Lett.* **2021**, *19*, 77−109.

(10) Mondal, M. K.; Balsora, H. K.; Varshney, P. Progress and trends in CO2 capture/separation technologies: A review. *Energy* **2012**, *46* (1), 431−441.

(11) Samanta, A.; Zhao, A.; Shimizu, G. K.; Sarkar, P.; Gupta, R. Post-combustion CO2 capture using solid sorbents: a review. *Ind. Eng. Chem. Res.* **2012**, *51* (4), 1438−1463.

(12) Lai, J. Y.; Ngu, L. H.; Hashim, S. S. A review of CO2 adsorbents performance for different carbon capture technology processes conditions. *Greenhouse Gases: Sci. Technol.* **2021**, *11* (5), 1076−1117.

(13) Sun, M.; Gu, Q.; Hanif, A.; Wang, T.; Shang, J. Transition metal cation-exchanged SSZ-13 zeolites for CO2 capture and separation from N2. *Chem. Eng. J.* **2019**, *370*, 1450−1458.

(14) Shang, S.; Tao, Z.; Yang, C.; Hanif, A.; Li, L.; Tsang, D. C. W.; Gu, Q.; Shang, J. Facile synthesis of CuBTC and its graphene oxide composites as efficient adsorbents for CO2 capture. *Chem. Eng. J.* **2020**, *393*, No. 124666.

(15) Hanif, A.; Dasgupta, S.; Nanoti, A. High temperature CO2 adsorption by mesoporous silica supported magnesium aluminum mixed oxide. *Chemical. Eng. J.* **2015**, *280*, 703−710.

(16) Hanif, A.; Sun, M.; Tao, Z.; Liu, L.; Tsang, D. C. W.; Gu, Q.; Shang, J. Silica supported MgO as an adsorbent for precombustion CO2 capture. *ACS Applied Nano Materials* **2019**, *2* (10), 6565−6574.
(17) Dissanayake, P. D.; You, S.; Igalavithana, A. D.; Xia, Y.; Bhatnagar, A.; Gupta, S.; Kua, H. W.; Kim, S.; Kwon, J. H.; Tsang, D. C. W.; Ok, Y. S. Biochar-based adsorbents for carbon dioxide capture: A critical review. *Renewable Sustainable Energy Rev.* **2020**, *119*, No. 109582.
(18) Sevilla, M.; Valle-Vigón, P.; Fuertes, A. B. N-doped polypyrrole-based porous carbons for CO2 capture. *Adv. Funct. Mater.* **2011**, *21* (14), 2781−2787.
(19) Xiao, J.; Yuan, X.; Zhang, T. C.; Ouyang, L.; Yuan, S. Nitrogen-doped porous carbon for excellent CO2 capture: A novel method for preparation and performance evaluation. *Sep. Purif. Technol.* **2022**, *298*, No. 121602.
(20) Li, Y.; Liu, L.; Yu, H.; Zhao, Y.; Dai, J.; Zhong, Y.; Pan, Z.; Yu, H. Synergy of developed micropores and electronic structure defects in carbon-doped boron nitride for CO2 capture. *Sci. Total Environ.* **2022**, *811*, No. 151384.
(21) Guo, L.; Yang, J.; Hu, G.; Hu, X.; Wang, L.; Dong, Y.; DaCosta, H.; Fan, M. Role of hydrogen peroxide preoxidizing on CO2 adsorption of nitrogen-doped carbons produced from coconut shell. *ACS Sustainable Chem. Eng.* **2016**, *4* (5), 2806−2813.
(22) Mohamedkhair, A. K.; Aziz, M. A.; Shah, S. S.; Shaikh, M. N.; Jamil, A. K.; Qasem, M. A. A.; Buliyaminu, I. A.; Yamani, Z. H. Effect of an activating agent on the physicochemical properties and supercapacitor performance of naturally nitrogen-enriched carbon derived from Albizia procera leaves. *Arab. J. Chem.* **2020**, *13* (7), 6161−6173.
(23) (a) Hanif, A.; Dasgupta, S.; Divekar, S.; Arya, A.; Garg, M. O.; Nanoti, A. A study on high temperature CO2 capture by improved hydrotalcite sorbents. *Chemical Engineering Journal* **2014**, *236*, 91−99. Hanif, A.; Dasgupta, S.; Nanoti, A. Facile synthesis of high-surface-area mesoporous MgO with excellent high-temperature CO2 adsorption potential. *Ind. Eng. Chem. Res.* **2016**, *55* (29), 8070−8078.
(24) Sun, M.; Zhu, X.; Wu, C.; Masek, O.; Wang, C. H.; Shang, J.; Ok, Y. S.; Tsang, D. C. W. Customizing high-performance molten salt biochar from wood waste for CO2/N2 separation. *Fuel Process. Technol.* **2022**, *234*, No. 107319.
(25) Vivo-Vilches, J. F.; Pérez-Cadenas, A. F.; Maldonado-Hódar, F. J.; Carrasco-Marín, F.; Faria, R. P. V.; Ribeiro, A. M.; Ferreira, A. F. P.; Rodrigues, A. E. Biogas upgrading by selective adsorption onto CO2 activated carbon from wood pellets. *J. Environ. Chem. Eng.* **2017**, *5* (2), 1386−1393.
(26) Guo, S.; Li, Y.; Wang, Y.; Wang, L.; Sun, Y.; Liu, L. Recent advances in biochar-based adsorbents for CO2 capture. *Carbon Capture Sci. Technol.* **2022**, *4*, No. 100059.
(27) Wang, J.; Wang, S. Preparation, modification and environmental application of biochar: A review. *J. Cleaner Prod.* **2019**, *227*, 1002−1022.
(28) (a) Hartman, M.; Svoboda, K.; Pohořelý, M.; Šyc, M. Thermal decomposition of sodium hydrogen carbonate and textural features of its calcines. *Ind. Eng. Chem. Res.* **2013**, *52* (31), 10619−10626. Wu, Y. L.; Shih, S. M. Intrinsic kinetics of the thermal decomposition of sodium bicarbonate. *Thermochim. Acta* **1993**, *223*, 177−186.
(29) Palaniselvam, T.; Aiyappa, H. B.; Kurungot, S. An efficient oxygen reduction electrocatalyst from graphene by simultaneously generating pores and nitrogen doped active sites. *J. Mater. Chem.* **2012**, *22* (45), 23799−23805.
(30) Kim, S. G.; Park, O. K.; Lee, J. H.; Ku, B. C. Layer-by-layer assembled graphene oxide films and barrier properties of thermally reduced graphene oxide membranes. *Carbon Lett.* **2013**, *14* (4), 247−250.
(31) Mojoudi, N.; Mirghaffari, N.; Soleimani, M.; Shariatmadari, H.; Belver, C.; Bedia, J. Phenol adsorption on high microporous activated carbons prepared from oily sludge: equilibrium, kinetic and thermodynamic studies. *Sci. Rep.* **2019**, *9* (1), 1−12.
(32) Peng, Y.; Sun, Y.; Hanif, A.; Shang, J.; Shen, Z.; Hou, D.; Zhou, Y.; Chen, Q.; Ok, Y. S.; Tsang, D. C. W. Design and fabrication of exfoliated Mg/Al layered double hydroxides on biochar support. *J. Cleaner Prod.* **2021**, *289*, No. 125142.
(33) Liu, Y.; Liu, X.; Dong, W.; Zhang, L.; Kong, Q.; Wang, W. Efficient adsorption of sulfamethazine onto modified activated carbon: a plausible adsorption mechanism. *Sci. Rep.* **2017**, *7* (1), 12437.
(34) Min, M.; Seo, S.; Yoon, Y.; Cho, K.; Lee, S. M.; Lee, T.; Lee, H. Catalyst-free bottom-up growth of graphene nanofeatures along with molecular templates on dielectric substrates. *Nanoscale* **2016**, *8* (38), 17022−17029.
(35) (a) Thommes, M.; Kaneko, K.; Neimark, A. V.; Olivier, J. P.; Rodriguez-Reinoso, F.; Rouquerol, J.; Sing, K. S. W. Physisorption of gases, with special reference to the evaluation of surface area and pore size distribution (IUPAC Technical Report). *Pure Appl. Chem.* **2015**, *87* (9−10), 1051−1069. Sing, K. S. W.; Williams, R. T. Physisorption hysteresis loops and the characterization of nanoporous materials. *Adsorp. Sci. Technol.* **2004**, *22* (10), 773−782.
(36) Zhu, X.; Sun, M.; Zhu, X.; Guo, W.; Luo, Z.; Cai, W.; Zhu, X. Molten salt shielded pyrolysis of biomass waste: Development of hierarchical biochar, salt recovery, CO2 adsorption. *Fuel* **2023**, *334*, No. 126565.
(37) Shang, S.; Yang, C.; Wang, C.; Qin, J.; Li, Y.; Gu, Q.; Shang, J. Transition-metal-containing porphyrin metal−organic frameworks as π-backbonding adsorbents for NO2 removal. *Angew. Chem., Int. Ed.* **2020**, *59* (44), 19680−19683.
(38) Xu, X.; Zheng, Y.; Gao, B.; Cao, X. N-doped biochar synthesized by a facile ball-milling method for enhanced sorption of CO2 and reactive red. *Chem. Eng. J.* **2019**, *368*, 564−572.
(39) Xiong, Z.; Shihong, Z.; Haiping, Y.; Tao, S.; Yingquan, C.; Hanping, C. Influence of NH 3/CO 2 modification on the characteristic of biochar and the CO 2 capture. *BioEnergy Res.* **2013**, *6*, 1147−1153.
(40) Manyà, J. J.; González, B.; Azuara, M.; Arner, G. Ultra-microporous adsorbents prepared from vine shoots-derived biochar with high CO2 uptake and CO2/N2 selectivity. *Chem. Eng. J.* **2018**, *345*, 631−639.
(41) Guo, Y.; Tan, C.; Sun, J.; Li, W.; Zhang, J.; Zhao, C. Biomass ash stabilized MgO adsorbents for CO2 capture application. *Fuel* **2020**, *259*, No. 116298.
(42) Gargiulo, V.; Gomis-Berenguer, A.; Giudicianni, P.; Ania, C. O.; Ragucci, R.; Alfè, M. Assessing the potential of biochars prepared by steam-assisted slow pyrolysis for CO2 adsorption and separation. *Energy Fuels* **2018**, *32* (10), 10218−10227.
(43) Cao, L.; Zhang, X.; Xu, Y.; Xiang, W.; Wang, R.; Ding, F.; Hong, P.; Gao, B. Straw and wood based biochar for CO2 capture: Adsorption performance and governing mechanisms. *Sep. Purif. Technol.* **2022**, *287*, No. 120592.
(44) Ji, Y.; Zhang, C.; Zhang, X.; Xie, P.; Wu, C.; Jiang, L. A high adsorption capacity bamboo biochar for CO2 capture for low temperature heat utilization. *Sep. Purif. Technol.* **2022**, *293*, No. 121131.

https://doi.org/10.1021/acsomega.3c04693
ACS Omega 2023, 8, 36228−36236